Icarus 215 (2011) 712–720

Contents lists available at SciVerse ScienceDirect

Icarus

journal homepage: www.elsevier.com/locate/icarus

On the dynamical stability of the very low-mass object Gliese 22 Bb

Manuel Andrade [a,b,*], José A. Docobo [a,c]

[a] Astronomical Observatory R. M. Aller, Universidade de Santiago de Compostela, 15782 Santiago de Compostela, Galiza, Spain
[b] Departamento de Matemática Aplicada, Escola Politécnica Superior, 27002 Lugo, Galiza, Spain
[c] Departamento de Matemática Aplicada, Facultade de Matemáticas, 15782 Santiago de Compostela, Galiza, Spain

ARTICLE INFO

Article history:
Received 1 December 2010
Revised 11 July 2011
Accepted 12 July 2011
Available online 23 July 2011

Keywords:
Extrasolar planets
Orbit determination
Planetary dynamics

ABSTRACT

Gliese 22 is a hierarchical triple red dwarf system formed by two close components, Aa and Ab, and a distant component, B, which is moving around the center of mass of the first two.

The possible existence of a fourth very low-mass object (15 Jupiter mass) orbiting around component B was reported by Docobo et al. (Docobo, J.A. et al. [2007]. IAU Commun. 26, 3–4). In this probable scenario with four bodies, component B would be in reality two: star Ba and the new object, Bb.

Two full three-dimensional accurate (circular and elliptical) solutions for the orbit of Bb have been obtained, along with an improved arrangement of the system masses. In addition, such a multiple system is analyzed by means of a (2 + 2)-body model considering its evolution during 10 Myr. In particular, we have studied its apsidal motion in order to eventually find any evidence of chaotic behavior. The nature of the new object as a giant planet or a brown star is also discussed.

1. Introduction

Gliese 22 (WDS 00321+6715, HIP 2552, ADS 440) is a hierarchical triple stellar system of red dwarfs located at approximately 10 parsecs. The two closest components within the system, Aa and Ab, move around their center of mass, CoM_A. These orbits are equivalent to the relative motion of Ab around Aa (hereafter, orbit Aa–Ab). Orbit Aa–Ab can be considered to be close to definitive keeping in mind that it was calculated on the basis of a set of very precise astrometric measurements (speckle interferograms) performed during one complete revolution of 15.64 years (Docobo et al., 2006). The most distant component, B, orbits around CoM_A in a little less than 225 years (hereafter, orbit A–B). This orbit is still preliminary but it was obtained after a rigorous selection as described below.

Of all of the orbits that fit the observations, we selected the one that yielded a total mass of $0.692 \pm 0.034\ M_\odot$, that is, the same mass that was obtained from empirical calibrations based on spectral types and magnitudes of the three components (Docobo et al., 2008).

The elements that define both orbits can be seen in Table 1, while Fig. 1 shows a mobile diagram that summarizes some system data. The two calculated orbits are co-revolving and practically co-planar with a mutual inclination of 2.°7.

A numerical integration extended over 10 Myr showed no evidence of secular changes in semimajor axes, eccentricities, nor inclinations. Therefore we concluded that, at least in the interval considered, the Gliese 22 stellar system is dynamically stable.

In addition, when we calculated the A–B orbit, we detected a weak sinusoidal pattern in the apparent motion of component B (see Fig. 2), that may be attributed to either a very unusual distribution of observational residuals or perhaps to an unseen fourth body in the system (Docobo et al., 2007, 2008). In the latter case, component B would consist of two bodies, the main one, star Ba, and a very low-mass object, Bb, that is about 15 times the mass of Jupiter ($15\ M_J$). Bb describes an orbit around Ba in 15 years (hereafter, Ba–Bb orbit). This proposed four-body system would be an unusual double-double hierarchy as compared to the multiple systems with planets that have been previously discovered.

This paper is structured as follows. After the Introduction (Section 1), a full three-dimensional accurate orbit (circular and elliptical versions) for the very low-mass object as well as its precise mass are given in Section 2. A discussion of its planetary or stellar nature is also presented as well as some comments about possibilities of detection by direct imaging and the ephemerides for the years in the next observation window. In Section 3, we present some results regarding the orbital stability of the four-body system, particularly those that refer to apsidal motion. Finally, conclusions and future research are discussed in Section 4.

* Corresponding author at: Departamento de Matemática Aplicada, Escola Politécnica Superior, 27002 Lugo, Galiza, Spain.
E-mail addresses: manuel.andrade@usc.es (M. Andrade), joseangel.docobo@usc.es (J.A. Docobo).

0019-1035/$ - see front matter © 2011 Elsevier Inc. All rights reserved.
doi:10.1016/j.icarus.2011.07.008

Table 1
Orbital elements for the Aa–Ab pair (Docobo et al., 2006) and the A–B pair (Docobo et al., 2008).

Orbital elements	Aa–Ab pair	A–B pair
P (yr)	15.64 ± 0.20	$223.3^{+7.2}_{-9.8}$
T	2000.76 ± 0.20	$1859.4^{+5.3}_{-2.4}$
e	0.174 ± 0.003	$0.293^{+0.044}_{-0.025}$
a (″)	0.511 ± 0.005	$3.322^{+0.040}_{-0.060}$
i (°)	44.6 ± 1.5	$47.3^{+0.5}_{-0.3}$
Ω (°)	175.1 ± 1.0	$174.9^{+2.7}_{-1.3}$
ω (°)	106.8 ± 5.0	$146.3^{+2.0}_{-3.8}$

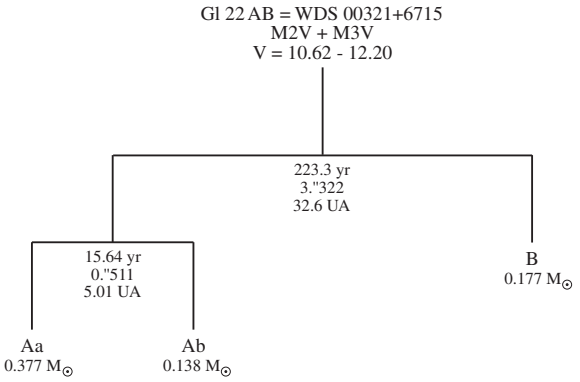

Fig. 1. Mobile diagram of the triple stellar system, Gl 22 AB.

2. Orbit, mass, and nature of the new companion, Bb

2.1. Orbital elements and masses

In a previous article (Andrade and Docobo, 2009), a set of preliminary elements of the fourth body was determined. At first, the orbit was considered to be circular. Nevertheless, a more detailed study of the observed sinusoidal trajectory showed that orbits with an eccentricity of up to 0.08 are possible because the residuals obtained are similar. Therefore, we consider the cases of minimum and maximum eccentricity: the circular solution (CS) and the elliptic solution (ES) with eccentricity of 0.08. The elements that define each of these orbits are shown in Table 2. In both cases the orbit of Bb around Ba is practically co-planar with the Aa–Ab and A–B orbits.

Table 2
Proposed sets of orbital elements for the Ba–Bb orbit.

Orbital elements	Circular solution (Andrade and Docobo, 2009)	Elliptic solution (this paper)
P (yr)	15 ± 2	15.0 ± 0.5
T	2010 ± 2	2010.0 ± 0.5
e	0 (assumed)	0.08 ± 0.05
a (″)	0.348 ± 0.010	0.348 ± 0.010
i (°)	46 ± 5	47.0 ± 5.0
Ω (°)	175 ± 5	175.0 ± 5.0
ω (°)	0 (assumed)	347.0 ± 5.0

Table 3
New arrangements of the masses.

	Masses	($M_\odot$)
	M	0.692 ± 0.034
Three bodies scenario	M_{Aa}	0.377 ± 0.030
(Docobo et al., 2008)	M_{Ab}	0.138 ± 0.007
	M_B	0.177 ± 0.014
Four bodies scenario	M_{Ba}	0.162 ± 0.014
Circular solution	M_{Bb}	0.0152 ± 0.0053
(Andrade and Docobo, 2009)		(=16.0 ± 5.6 M_J)
Four bodies scenario	M_{Ba}	0.162 ± 0.014
Elliptic solution	M_{Bb}	0.0147 ± 0.0027
(this paper)		(=15.4 ± 2.8 M_J)

Using the subindices 1, 2 and 3 in order to refer to the Aa–Ab, A–B, and Ba–Bb orbits, respectively, the values of the mutual inclinations are the following: $i_{13} = 1.°4$, $i_{23} = 1.°3$, in the case of CS, and $i_{13} = 2.°4$, $i_{23} = 0.°4$, in the case of ES.

Considering the value of the parallax given by Docobo et al. (2008), 102 ± 1 mas, we estimate that Bb is located at 3.41 ± 0.10 AU from its closest stellar companion, Ba.

On the other hand, the total mass of 0.692 ± 0.034 $M_\odot$ is distributed in the manner represented in Table 3. The mass of the possible fourth body varies slightly if its orbit is considered to be elliptic, but the two cases are similar.

2.2. Extrasolar planet or brown dwarf?

Despite attempts to clarify the differences, there are no universally accepted criteria to distinguish giant planets from brown dwarfs. One of the most widely accepted condition is known as the deuterium-burning mass limit criterion which estimates the

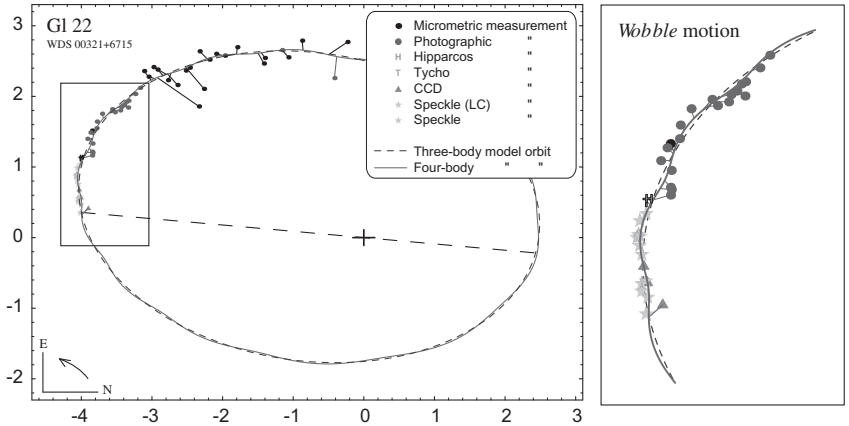

Fig. 2. Left: the apparent orbit of component B relative to the center of mass of Aa–Ab (the scale on both axes is in arc seconds). Each measurement (see legend) is connected to its predicted position by an *O–C* line. The dashed line passing through the primary star is the line of nodes and the arrow shows the direction of the orbital motion. Right: zoom of the orbit showing the wobble motion of the B component due to the possible new object in the area of measurements with the highest weight (Docobo et al., 2008).

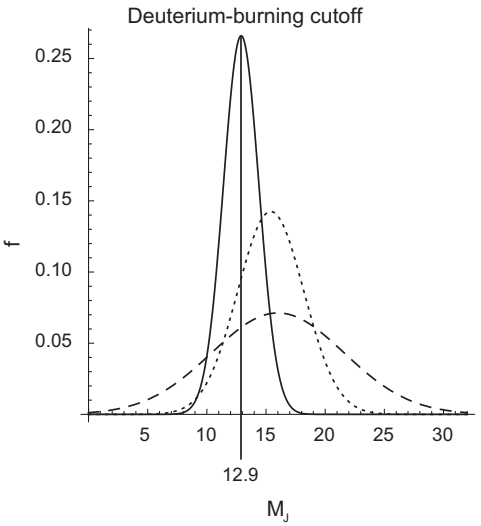

Fig. 3. Probability density functions corresponding to the deuterium-burning mass limit (solid line) and to the masses of the Bb component obtained from the circular solution (dashed line) and from the elliptic solution (dotted line).

Table 4
Probability of planetary or stellar nature for the Bb companion according to the deuterium-burning mass limit criterion depending on metallicity (abbreviated as metall.).

Solution	Nature	Probability (%)		
		Low metall.	Mean metall.	High metall.
Circular	Planet	39	29	20
	Brown dwarf	61	71	80
Elliptic	Planet	36	19	8
	Brown dwarf	64	81	92

mass to fuse deuterium to be 12.9 ± 1.5 M_J (see Spiegel et al. (2011) for a detailed discussion). This value has been recognized as the threshold for transition from planets to brown dwarfs. Another criterion establishes such a delineation according to the object's origin and formation; around 13 M_J, there are bodies with stellar and planetary characteristics (Spiegel et al., 2011).

In the system studied here, the mass of the Bb companion varies according to the chosen orbital solution: 16.0 ± 5.6 M_J (CS) or 15.4 ± 2.8 M_J (ES). Assuming a normal distribution for these uncertainties and considering their corresponding probability density functions as given by Fig. 3, we can statistically estimate in each case the probability of the companion mass being below or above the deuterium-burning cutoff (see Table 4).

Accordingly, the Bb object would more probably be a very low-mass brown dwarf. However, these results are not yet conclusive. The actual deuterium-burning cutoff is extremely sensitive to metallicity through its influence on atmospheric opacity so that greater metallicity leads to deuterium burning at lower mass and, conversely, lesser metallicity leads to deuterium burning at higher mass. In fact, we estimate such probabilities taking into account gradations of this from 2-times the solar metallicity (high) to a fraction of the solar metallicity (low) according to Spiegel et al. (2011).

Moreover, the second criterion in differentiating a planet from a brown dwarf, that is, by their mode of formation, could lead to support either possibility. From this point of view, brown dwarfs form by condensations in an interstellar gas cloud (in the same way as stars) whereas planets accrete from material in a circumstellar disk. In our opinion, more astrophysical data about the origin of the companion in comparison with the three stellar components of the system is needed in order to arrive at a reliable conclusion.

Table 5
Ephemerides for both solutions of the Ba–Bb orbit during the next observation window.

Epoch	Circular solution		Elliptic solution	
	θ (°)	ρ (″)	θ (°)	ρ (″)
2016	328.2	0.315	321.6	0.320
2017	346.6	0.344	338.7	0.359
2018	3.4	0.344	353.1	0.375
2019	21.8	0.315	7.5	0.362
2020	45.3	0.272	24.3	0.322

2.3. Prospects for the direct detection of the Bb object

Several extrasolar planets have been detected by direct imaging since the first successful direct detection of a planetary mass companion orbiting a brown dwarf with VLT (Chauvin et al., 2004). However, the direct imaging of extrasolar planets and, ultimately, their spectroscopic study around normal stars (not brown dwarfs) remains a difficult task even when using outstanding instrumentation. Nevertheless in the last few years a very promising technique that combines a stellar coronagraph with adaptive optics on ground-based telescopes has enabled observers to find new planets around nearby stars. For example, the Gemini Planet Imager (GPI), a coronagraphic instrument designed to detect companions by imaging, is capable of perceiving the flux of faint companions near a much brighter host star with detectable contrast ratios of 10^7. Observations are made within a region delimited by the radius of the occulting disk of the coronagraph (0.″22) and a concentric square of 2.″8 × 2.″8 (Kataria and Simon, 2010).

The small distance to the host star (3.41 ± 0.10 AU) is certainly a drawback in the Gl 22 Bb case. On the contrary, the moderate brightness of the M3V star and the relatively large size of the companion could provide an opportunity to directly detect the latter by means of techniques such as the above-mentioned. Taking into account both orbital solutions given in this paper, we have calculated angular separations and position angles of the Bb object with respect to the Ba stellar component for the coming years up to completion of an orbital period. Considering the GPI coronagraph, the next best observation window will take place between 2016 and 2020 (see Table 5) with separations above 0.″3 for both solutions (see Fig. 4). The maximum value will be 0.″35 in the middle of 2017 for the circular solution and 0.″38 at the beginning of 2018 for the elliptic one. Nevertheless, due to the small eccentricity, minimum separation will never be below 0.″24, which will occur in the middle of 2013 for the circular solution and at the end of 2013 for the elliptic one. We must note that, because of the lack of radial velocities, we cannot determine which is the ascending node and consequently in what parts of the observation window the Bb object will be in quarter phase or greater (the most propitious case for a positive detection).

Thus, according to previous contributions concerning the utility of astrometry as a precursor to direct detection (Savransky et al., 2009; Davidson, 2011), this astrometric orbit of Gl 22 Bb permits the planning and scheduling of a sequence of imaging observations to directly detect this very low-mass object. The completion of this goal would allow us to independently calculate the semimajor axis, eccentricity, and orbital inclination. It could be crucial to specify the planet's true mass and, therefore, to unambiguously determine its stellar or planetary nature. In addition, it would provide the possibility of determining the colors and spectra of Gl 22 Bb.

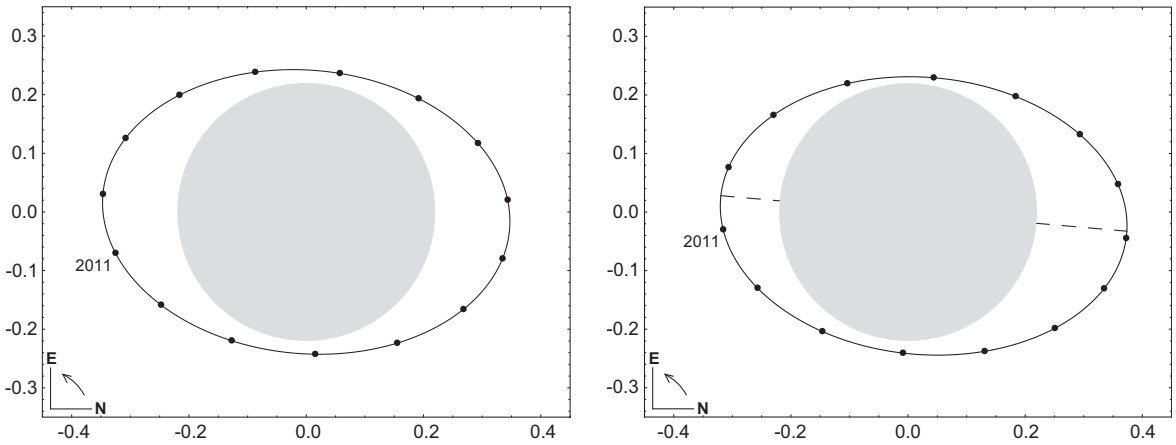

Fig. 4. Apparent orbit (left: circular solution; right: elliptic solution) for the Gl 22 Bb (scale is in arc seconds). Positions at the beginning of each year during one orbital period from 2011 onward are indicated by black points. The dashed line is the line of nodes. As an example, we have drawn a gray disk which shows the radius (0.″22) of the occulting disk of the GPI coronagraph.

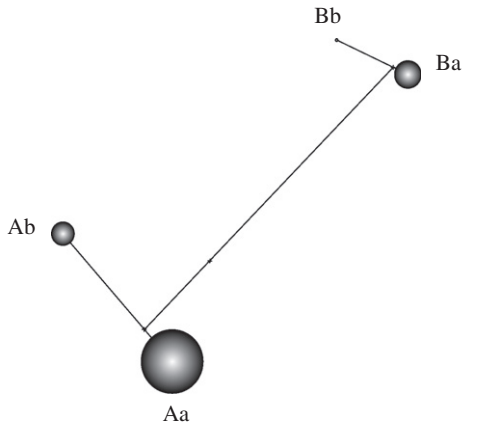

Fig. 5. Jacobian coordinate system (distances and sizes are not to scale).

3. Dynamical analysis of the Ba–Bb orbit

3.1. Orbital stability

In order to give a complete description of this system, we have considered the double 4(2,2) model of the four-body problem where a hierarchical pair of binaries is revolving around their common center of mass. In addition, we have taken the generalized Jacobi coordinated system shown in Fig. 5.

With the objective of investigating the further evolution of the system including the Bb object, we have integrated the hierarchical (nearly-Keplerian) four-body system for the two considered orbital solutions. This task has been carried out by means of an implicit Runge–Kutta integrator performed by using the *Mathematica* package. This class of methods has many desirable properties such as stability and efficiency. In this case we have implemented an integrator with a variable-step size in order to minimize the local error per step, over spans of one period of the Ba–Bb orbit (15 years). As a result, all integrations conserve energy and angular momentum to better than 10^{-9} and 10^{-4}, respectively.

An exploration of the orbital elements and the parameter space in 10 Myr integrations shows that neither semimajor axes nor eccentricities exhibit secular variations in either case. Nevertheless, a non-regular periodic evolution of eccentricity of the new companion is observed. With respect to this and independent of its initial value, eccentricity tends to oscillate around a similar mean value, 0.04 in the case of the circular solution and 0.05 for the elliptic solution. This suggests that the most probable solution should not be exactly circular. We can see the evolution of the orbital eccentricities with their periodic variations in Fig. 6.

Integrations show that all orbital elements undergo relatively small periodical variations (see Table 6) except for the arguments of periastra and the times of periastron passages that advance secularly. On the other hand, the mutual inclinations remain approximately constant with maximum periodical variations as small as $\Delta i_{12} = 0.^\circ3$, $\Delta i_{23} = 1.^\circ4$ (circular solution) and $\Delta i_{12} = 0.^\circ2$, $\Delta i_{23} = 1.^\circ5$ (elliptic solution) for the considered interval.

Another approach takes advantage of the empirical expression developed by Holman and Wiegert (1999) to determine the maximum value of the semimajor axis of the stable orbit of an extrasolar planet in a stellar binary system (see Eq. (1) in Holman and Wiegert (1999)).

It is important to note that this formula was obtained based on the results of numerical simulations of an elliptic three-body system. Thus, in order to roughly estimate the critical semimajor axis, we see this formula taking into account the following considerations: (i) the mass of the Bb object is sufficiently small so that it does not significantly perturb stellar components (it is only 2% of the total mass), and (ii) we assume the Aa–Ab pair mass is concentrated at the center of mass. Considering uncertainties of the orbital elements (see the last column in Table 1), we obtain the following critical semimajor axis:

$$a_c = 0.''401^{+0.''076}_{-0.''071} (\simeq 3.93^{+0.75}_{-0.70}\mathrm{AU}).$$

Comparing this result with the estimated value of the semimajor axis of the Ba–Bb orbit, $a = 0.''348 \pm 0.''010$ ($\simeq$3.41 ± 0.10 AU), we notice that $a < a_c$ indicating that the orbit of the new pair Ba–Bb is stable. However, the large uncertainty in the critical semimajor axis could lead to other scenarios. In fact, assuming a normal distribution for these uncertainties and considering the corresponding probability density functions (see Fig. 7), we estimate that the probability of a critical value below the mean value is a significant 22.8%.

3.2. Apsidal motion

The analysis of the displacements of the semimajor axes (apsidal motion) is usually a helpful tool to determine the dynamical stability in multiple planetary systems. It is well known that, in general, various types of apsidal behavior can be observed in this type of system: aligned libration, antialigned libration,

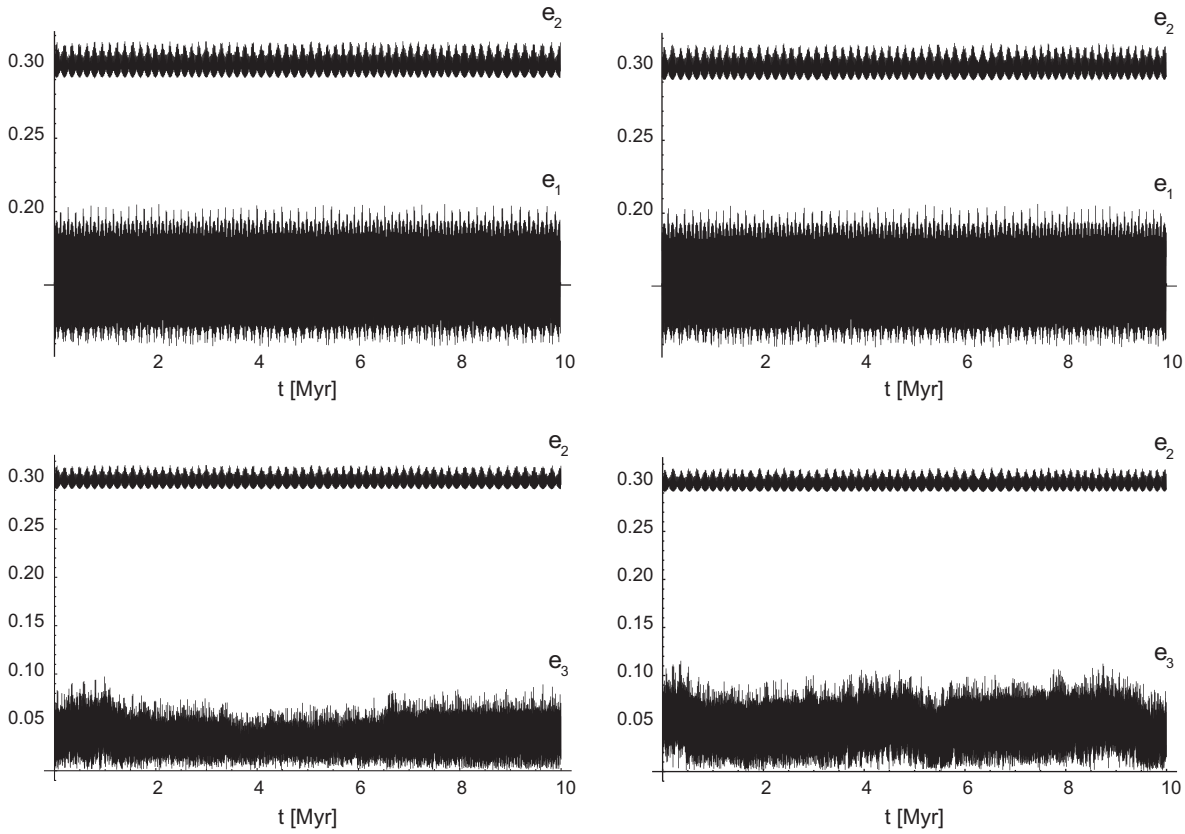

Fig. 6. Evolution of the orbital eccentricities for the circular solution (left) and the elliptic solution (right) during 10 Myr. Up: A–B and Aa–Ab orbits. Down: A–B and Ba–Bb orbits.

Table 6
The range of periodic variations of orbital elements at the end of 10 Myr. Note that "s" indicates secular evolution.

Solution	Pair	Orbital elements						
		ΔP (yr)	ΔT (yr)	Δe	Δa (AU)	Δi (°)	$\Delta\Omega$ (°)	$\Delta\omega$ (°)
Circular	Aa–Ab	0.5	s	0.097	0.099	4.4	6.0	s
	A–B	5.0	s	0.025	0.489	1.2	1.6	s
	Ba–Bb	1.1	s	0.097	0.171	6.1	8.4	s
Elliptic	Aa–Ab	0.5	s	0.098	0.097	4.5	6.1	s
	A–B	5.3	s	0.026	0.511	1.2	1.6	s
	Ba–Bb	1.2	s	0.115	0.175	4.4	6.0	s

nonsymmetric libration, circulation, near-separatrix motion between circulation and libration, or near-separatrix motion between modes of circulation (Barnes and Greenberg, 2006a). In our system the apsidal motion can be easily identified by considering the motion in a plane-polar coordinate system in terms of the so-called eccentricity vectors ($e_i e_j \cos\varpi_{ij}$, $e_i e_j \sin\varpi_{ij}$), where e_i and e_j are the eccentricities of i and j components and ϖ_{ij} is the difference in the longitudes of the periastra. Essentially, if the trajectory encompasses the origin, the system is circulating. Otherwise, it will be librating. In the latter case, if the trajectory lies entirely in the region where $e_i e_j \cos\varpi_{ij}$ is positive, the system is in aligned libration, whereas if it lies entirely in the negative region, the system is in antialigned libration. Moreover, if the polar trajectory passes close to the origin, the behavior will be more of the type *near separatrix*, between the circulation and libration behaviors.

The apsidal behavior of Gl 22 AB is analyzed by monitoring the aforementioned orbital elements over 10 Myr for each pair of adjacent orbits. In the case of the Aa–Ab and the A–B orbits, the numerical results clearly show circulation as much in the circular solution as in the elliptic one (see the upper part in Fig. 8).

In contrast, when we examine the case of the A–B and Ba–Bb orbits, no conclusion is obvious since the trajectory does not show a regular pattern. As regards the circular solution, it seems that the system is in an antialigned configuration but very close to the separatrix between antialigned libration and circulation; in fact, the distance from the origin is very small (see the lower left part in Fig. 8). This complex configuration probably arises because of the circularity of the Ba–Bb orbit whose most noticeable consequence is that the orientation of the major axis is not well defined so it can undergo very large changes. In contrast with this, a minor tendency to circulation appears as slightly preferable in the case of the elliptic solution (see the lower right part in Fig. 8).

The behavior of apsidal motion is more clearly recognizable in the phase-plane, ϖ_{23}–e_3, shown in Fig. 9. We can see that the circular solution shows libration of $\varpi_2 - \varpi_3$ about 180° (antialignment) whereas the elliptic one is most likely in a mixed configuration between circulation and libration. Apart from this, both solutions exhibit relatively small amplitude variations of e_3.

An alternative procedure that can help to decide whether an orbit is librating or circulating is the Zhou and Sun's index (Zhou and

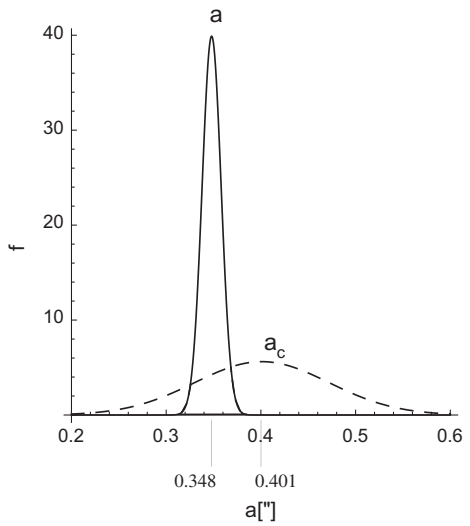

Fig. 7. Overlapping of the probability density functions corresponding to the estimated semimajor axis of the Ba–Bb orbit (solid line) and to the critical semimajor axis (dashed line).

Sun, 2003). An index, I_n, is defined to be computed every certain amount of time according to: $I_n = 0$ if $-\frac{\pi}{2} < \Delta\varpi < \frac{\pi}{2}$ and $I_n = 1$ if $\frac{\pi}{2} < \Delta\varpi < \frac{3\pi}{2}$. Thus, the average of all the I_n over a very large n, denoted by $\langle I_n \rangle$, will distinguish the apsidal configuration:

$$\langle I_n \rangle \approx \begin{cases} 0 & \text{aligned libration} \\ 0.5 & \text{circulation} \\ 1 & \text{antialigned libration} \\ \text{others} & \text{mixed} \end{cases}$$

In this case, we have computed this index over 10 Myr every 15 yr (one period of the Ba–Bb orbit). The results obtained for each orbit are shown in Table 7. In conformity with the conclusions obtained from the trajectories in the $(e_i e_j \cos\varpi_{ij}, e_i e_j \sin\varpi_{ij})$ plane, the apsidal motion of the Aa–Ab and the A–B orbits would be approximately in the circulating region for both solutions (circular and elliptic), in spite of a minor trend to the aligned libration region as $\langle I_n \rangle_{12} = 0.42$. Regarding the A–B and the Ba–Bb orbits, its apsidal motion would be virtually in the antialigned libration region ($\langle I_n \rangle_{23} = 0.91$) for the circular solution, whereas this behavior should tend to be in a mixed configuration between the circulation and the antialigned libration regions ($\langle I_n \rangle_{23} = 0.76$) in the case of the elliptic solution.

In order to confirm this behavior, we have also calculated the distribution function given by Barnes and Quinn (2004) in the following manner: $\Lambda = |\varpi_i - \varpi_j|$ if $\Lambda < \pi$ and $\Lambda = 360 - |\varpi_i - \varpi_j|$ if $\Lambda > \pi$, with i and j representing the components.

With respect to the Aa–Ab and the A–B orbits, the obtained results indicate that Λ is roughly circulating for both solutions. The average of all values of Λ over time, denoted by $\langle \Lambda \rangle$, is shown for each pair in Table 7. Also, histograms with all the values over time are shown in Fig. 10.

In contrast, for the most complex case of the A–B and the Ba–Bb orbits, Λ seems to prefer antialignment in the case of the circular solution ($\langle \Lambda \rangle_{23} \sim 140°$). On the other hand, when we analyze the case of the elliptic solution, we see that Λ seems to be circulating in spite of showing a pronounced trend to be antialigned (compare lower left and right parts in Fig. 10). This alternating between libration about antialignment and circulation results in the chaotic evolution of e_3 through ϖ_{23}–e_3 coupling, the same behavior observed in Fig. 6. Such process, connected to the weakening of the antialigned configuration, suggests that the eccentricity of the Ba–Bb orbit could begin to increase at some time and the system would become unstable on long timescales.

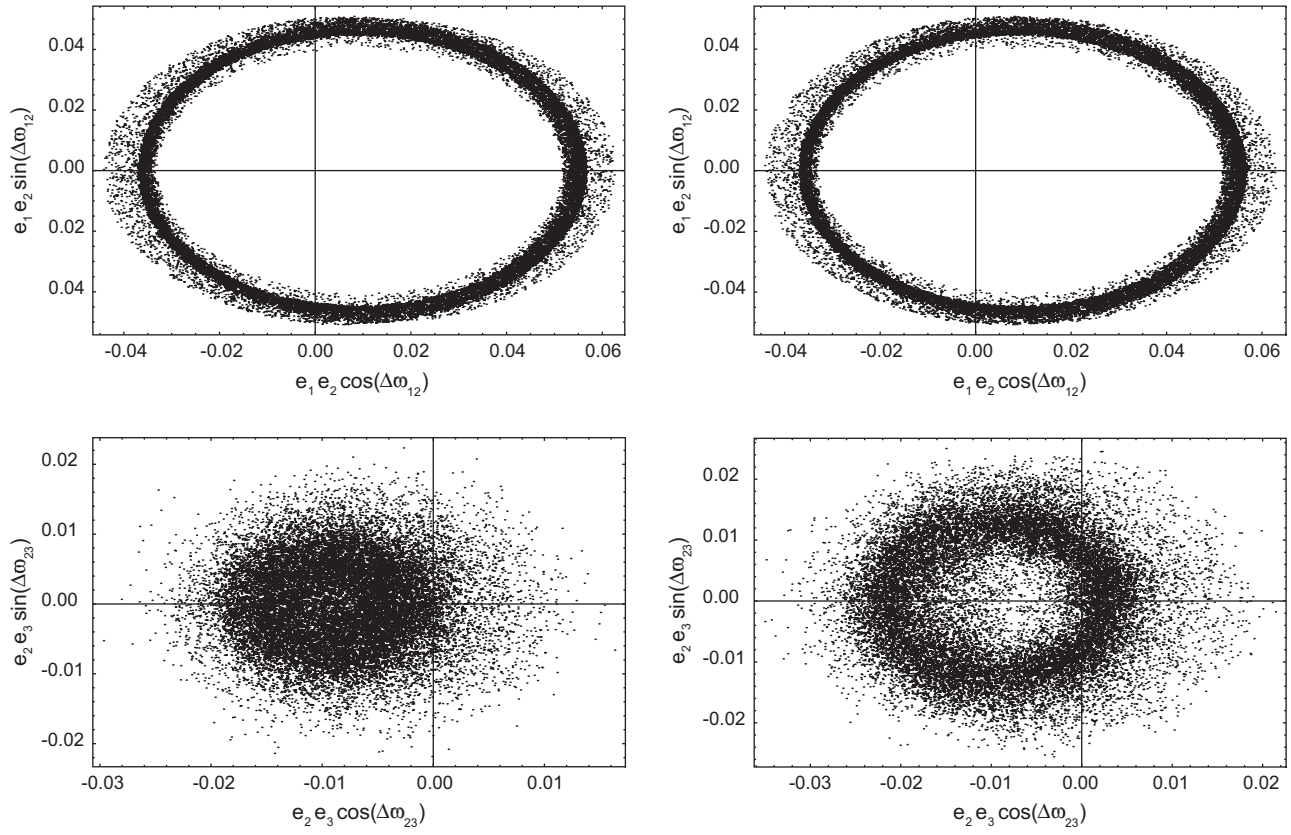

Fig. 8. Apsidal motion defined by points that represent the system at 15 yr intervals during 10 Myr for the circular solution (left) and the elliptic solution (right). Above: the A–B and the Aa–Ab orbits. Below: the A–B and the Ba–Bb orbits.

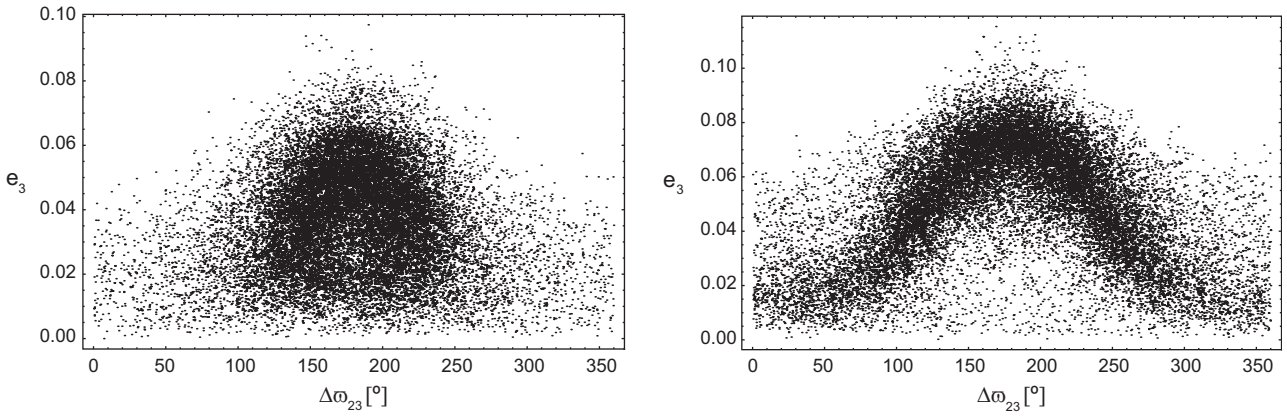

Fig. 9. The phase plane ϖ_{23}–e_3 defined by points that represent the system at 15 yr intervals during 10 Myr for the circular solution (left) and the elliptic solution (right).

Table 7
Zhou and Sun's index $\langle I_n \rangle$ and average Λ.

Solution	Pair	$\langle I_n \rangle$	$\langle \Lambda \rangle$ (°)
Circular	Aa–Ab/A–B	0.42	81.1
	Ba–Bb/A–B	0.91	140.0
Elliptic	Aa–Ab/A–B	0.42	81.0
	Ba–Bb/A–B	0.76	118.0

To explore this seemingly near-separatrix motion, we would take advantage of the fact that if a system is near a separatrix, the eccentricity periodically passes near zero. In this way, Barnes and Greenberg (2006b) defined the following parameter depending on the closest approach to the origin (numerator) and the scale of the trajectory (denominator):

$$\epsilon \sim \frac{2 \min\left(\sqrt{x^2+y^2}\right)}{(x_{max}-x_{min})+(y_{max}-y_{min})}$$

with x and y being the Cartesian coordinates in the plane-polar coordinate system: $x \equiv e_i e_j \cos \varpi_{ij}$ and $y \equiv e_i e_j \sin \varpi_{ij}$. If ϵ is small (less than a critical value, ϵ_{crit}), then the system lies near some type of separatrix. According to the authors, the results are not strongly dependent on the choice for ϵ_{crit}. For practical purposes it can be taken as $\epsilon_{crit} \sim 0.01$ or even $\epsilon_{crit} \sim 0.1$. After applying this test to our problem, we obtain $\epsilon_{CS} \simeq 0.013$ and $\epsilon_{ES} \simeq 0.005$ for circular and elliptic solutions, respectively. This would confirm that behavior is close to the libration–circulation separatrix in both cases.

Regarding an eventual interaction between Aa–Ab and Ba–Bb orbits, we have seen that the relative apsidal motion is dominated

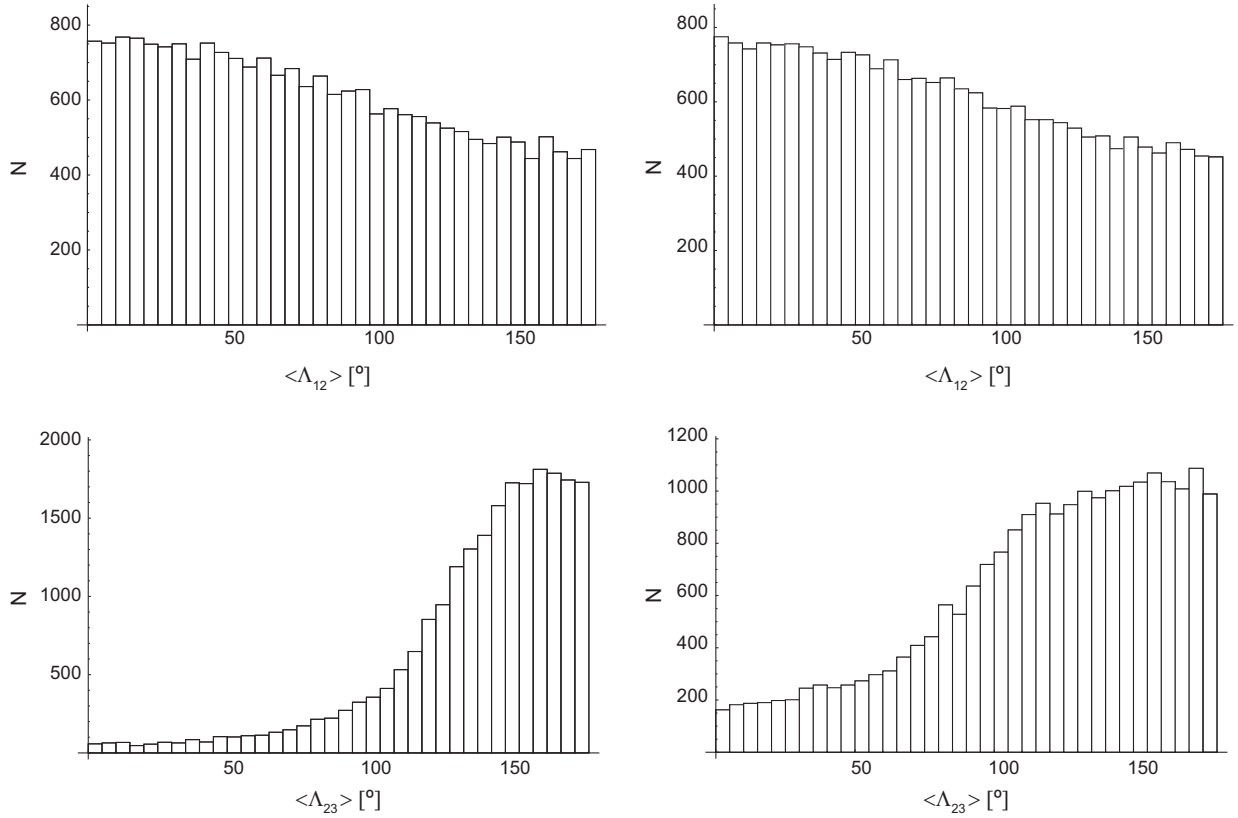

Fig. 10. The Λ distribution function for the circular solution (left) and the elliptic solution (right). Above: the Aa–Ab and the A–B orbits. Below: the A–B and the Ba–Bb orbits.

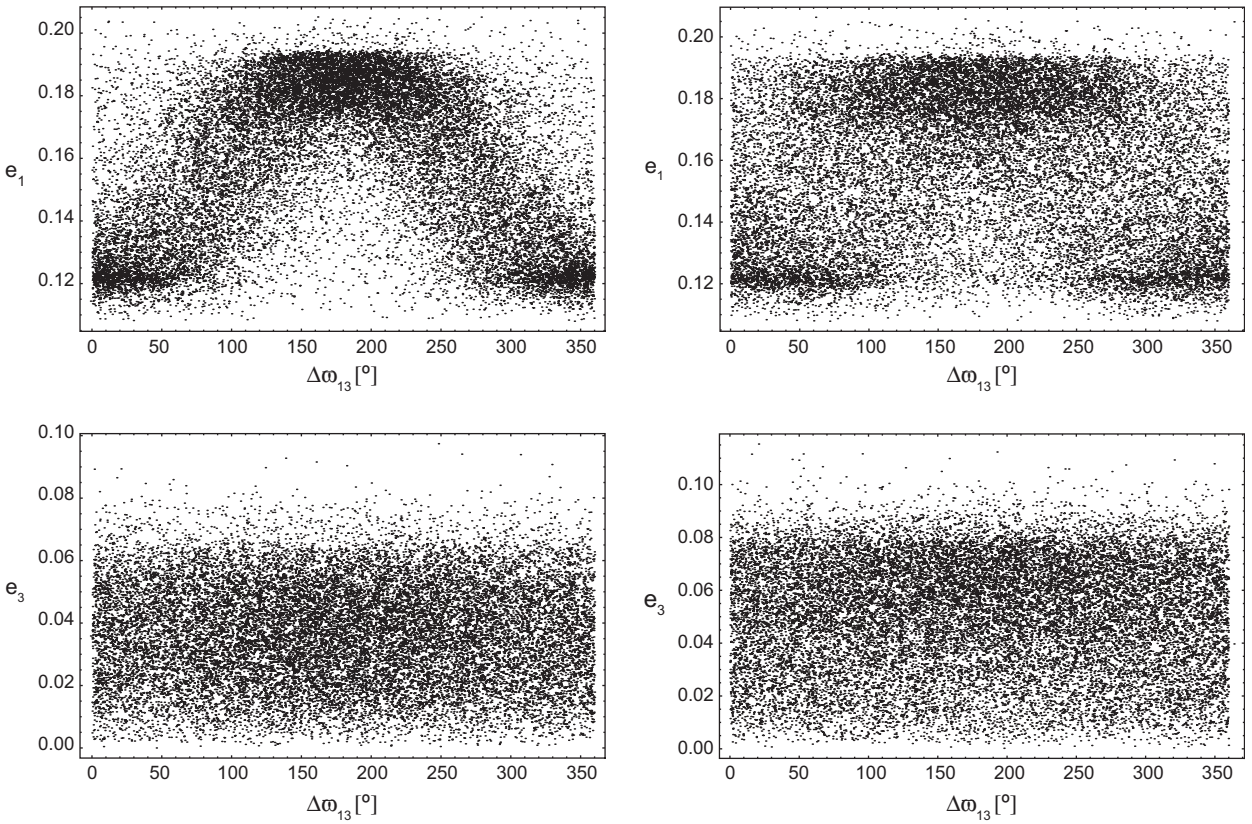

Fig. 11. The phase planes ϖ_{13}–e_1 (above) and ϖ_{13}–e_3 (below) defined by points that represent the system at 15 yr intervals during 10 Myr for the circular solution (left) and the elliptic solution (right).

by the periastron passages of the A–B orbit so that antialigned librations appear to be distributed superimposed over the circulation with a period similar to that of the A–B orbit. This non-regular coupled behavior about antialigned libration evolves towards a chaotic circulation if eccentricity and semimajor axis of the Ba–Bb orbit are increased. In fact, in the case of the circular solution, the Aa–Ab orbit reaches the highest values of eccentricity when its apside is antialigned with that of the Ba–Bb orbit, avoiding in this way frequent close encounters between both bodies. However, such a mechanism is considerably weakened in the case of the elliptic solution (see Fig. 11).

4. Conclusions

Two sets of orbital elements with their uncertainties were obtained for the new very-low mass object, Gl 22 Bb, after minimizing the RMS of the apparent orbit of the B component. The only essential difference between those solutions is the value of their eccentricities so that one solution is, initially, exactly circular whereas the other one is slightly elliptic. In addition, new and accurate arrangements of the masses were done for each solution distributing the mass between the third stellar component and the new companion.

The application of an implicit Runge–Kutta integrator extended over 10 Myr allows us to conclude that the four-body system, Gliese 22, is stable at least on that timescale in both circular and elliptic cases, since no significant secular changes in semimajor axes, eccentricities, nor inclinations were detected. Nevertheless, a slightly chaotic evolution of the eccentricity of the Ba–Bb orbit has been observed. Such behavior is confirmed by the analysis of the apsidal motion. We demonstrate that semimajor axes of the Aa–Ab and the A–B orbits are clearly circulating despite the fact that a minor trend toward alignment is observed. On the contrary, the behavior of the Ba–Bb orbit is much more complex. When we consider the circular solution, the system seems to be in librating region about antialignment, but very close to the separatrix between that and the circulating region. On the other hand, elliptic solution exhibits a mixed configuration between circulation and libration as well. This preference for antialignment could act as a mechanism to keep the system from breaking apart in the case of the circular solution. Such an effect would be somewhat weakened in the case of considering a slightly elliptic solution. In any case, small variations of semimajor axes and eccentricities suggest that this system can be considered to be stable in both cases, at least on the 10 Myr timescale.

Our numerical simulations of the Gliese 22 multiple system show that the Aa–Ab pair has a significant influence on the motion of the companion object. Such an action is stronger for larger initial values of the eccentricity and semimajor axis of Ba–Bb. Actually, further numerical experiments with values of the eccentricities and semimajor axes increased up to 3σ (or more) show a new phenomenon, a chaotic circulation of their apsides.

Concerning the planetary or stellar nature of this object, it is very difficult to make conclusions about it without more astrophysical data regarding composition and origin. Such observations should be accompanied by the use of high resolution techniques in order to refine the orbital elements of the Ba–Bb orbit as well as their uncertainties with the aim of obtaining a still more accurate companion mass. Possibly, in a few years, new coronagraphic instruments combined with adaptive optics could take advantage of the observation window expected from 2016 to 2020 and accomplish this goal.

Acknowledgments

This work has been supported by the Research Project, AYA 2010-18433, of the Spanish *Ministerio de Educación y Ciencia*. We are grateful to the anonymous reviewers for their valuable comments and suggestions which have led to improvements in this article.

References

Andrade, M., Docobo, J.A., 2009. Long-term stability for the Bb planetary-like object in the triple stellar system Gl 22. Monogr. R. Acad. Cienc. Zaragoza 32, 65–73.

Barnes, R., Greenberg, R., 2006a. Extrasolar planetary systems near a secular separatrix. Astrophys. J. 638, L478–L487.

Barnes, R., Greenberg, R., 2006b. Behavior of apsidal orientations in planetary systems. Astrophys. J. 652, L53–L56.

Barnes, R., Quinn, T., 2004. The (in)stability of planetary systems. Astrophys. J. 611, 494–516.

Chauvin, G. et al., 2004. A giant planet candidate near a young brown dwarf. Direct VLT/NACO observations using IR wavefront sensing. Astron. Astrophys. 425, L29–L32.

Davidson, J.M., 2011. Utilizing astrometric orbits to obtain coronagraphic images of extrasolar planets. Publ. Astron. Soc. Pacific 123 (906).

Docobo, J.A., Tamazian, V.S., Balega, Y.Y., Melikian, N.D., 2006. Speckle measurements and differential photometry of visual binaries with the 6 meter telescope of the special astrophysical observatory. Astron. J. 132, 994–998.

Docobo, J.A. et al., 2007. On the possible existence of a very low-mass object in the triple stellar system Gliese 22 (HIP 2552). IAU Commun. 26 (162), 3–4.

Docobo, J.A. et al., 2008. A methodology for studying physical and dynamical properties of multiple stars. Application to the system of red dwarfs Gl 22. Astron. Astrophys. 478, 187–191.

Holman, M.J., Wiegert, P.A., 1999. Long-term stability of planets in binary systems. Astron. J. 117, 621–628.

Kataria, T., Simon, M., 2010. Detectability of exoplanets in the β Pic Moving Group with the Gemini Planet Imager. Astron. J. 140, 206–214.

Savransky, D., Kasdin, N.J., Belson, B.A., 2009. The utility of astrometry as a precursor to direct detection. Proc. SPIE 7440, 0B1–0B9.

Spiegel, D.S., Burrows, A., Milsom, J.A., 2011. The deuterium-burning mass limit for brown dwarfs and giant planets. Astrophys. J. 727, 57–65.

Zhou, J.-L., Sun, Y.-S., 2003. Occurrence and stability of apsidal resonance in multiple planetary systems. Astrophys. J. 598, 1290–1300.